Journal of Power Sources 236 (2013) 17–24

Contents lists available at SciVerse ScienceDirect

Journal of Power Sources

journal homepage: www.elsevier.com/locate/jpowsour

Performance degradation of a direct borohydride fuel cell

Z.P. Li [a,*], Z.X. Liu [a], H.Y. Qin [a], K.N. Zhu [a], B.H. Liu [b]

[a] Department of Chemical and Biological Engineering, Zhejiang University, Hangzhou 310027, People's Republic of China
[b] Department of Materials Science and Engineering, Zhejiang University, Hangzhou 310027, People's Republic of China

HIGHLIGHTS

- Catalyst erosion from anode substrate is a major cause of performance degradation of the direct borohydride fuel cell.
- Cooperative interaction among Co, N, and C contributes to the good performance stability of $Co(OH)_2$–PPY/BP.
- $Co(OH)_2$ and CoOOH in $Co(OH)_2$–PPY/BP disappear after long time of operation.

ARTICLE INFO

Article history:
Received 12 September 2012
Received in revised form
21 January 2013
Accepted 22 January 2013
Available online 24 February 2013

Keywords:
Direct borohydride fuel cell
Performance degradation
Hydrogen evolution
Hydrophobic anode
Electrode polarization
Cooperative interaction

ABSTRACT

This study explores the performance degradation mechanism of direct borohydride fuel cells (DBFCs) by investigating the catalyst surface characteristics, electrode structure, and electrode polarization after cell operation. Catalyst erosion from the anode substrate is a major cause of DBFC performance degradation. The depression of hydrogen evolution effectively stabilizes DBFC performance. DBFCs using Ni–Pd/C as the anode catalyst and polypyrrole-modified carbon-supported $Co(OH)_2$ [$Co(OH)_2$–PPy/BP] as the cathode catalyst exhibit high performance stability. The performance stability of $Co(OH)_2$–PPy/BP is similar to that of commercial Pt/C, although only a small amount of Co remains after operation. The cooperative interaction among Co, N from polypyrrole, and C from the carbon supporter plays a very important role in the performance stability of a DBFC cathode.

1. Introduction

Direct borohydride fuel cells (DBFCs) are an emerging type of fuel cell that uses alkaline borohydride solutions as fuel [1,2]. DBFCs are attracting interest as a potential power source because of their high electromotive force of 1.64 V and high theoretical energy density (9.3 Wh g^{-1} of $NaBH_4$). Most recent studies have aimed at improving cell performance and depressing hydrogen evolution [1–3]. However, little attention has been paid to the performance stability of DBFCs, particularly to their long-term performance stability.

Generally, the performance degradation of a fuel cell is characterized by one of four loss mechanisms: (a) ohmic, (b) activation, (c) mass transportation, and (d) fuel efficiency losses. Performance degradation is usually caused by a combination of these losses. Hydrogen evolution in a DBFC is susceptible to performance degradation because hydrogen bubbles generated during operation block the anolyte flow in the channels of a bipolar plate (in short-term cell performance deterioration) [4–7] and erode catalyst particles away from the anode (in long-term cell performance deterioration). A three-dimensional Os anode has been developed to prevent catalyst erosion and improve the durability of DBFC anodes [8]. A special anode structure with upper and lower parts for the electrooxidation of borohydride [9] may be used to decrease the effects of hydrogen evolution on catalyst erosion.

Apart from hydrogen evolution at the anode, the anolyte crossover, hydrophobic characteristics of cathode, and nature of cathode catalyst also affect the performance stability of DBFCs [10,11]. Pt/C has higher electroactivity toward oxygen reduction reaction (ORR), as well as better performance stability, than Pd/C, Ag/C, and Ni/C [10]. Some non-precious catalysts such as iron tetramethoxyphenyl porphyrin have high borohydride tolerance, exhibiting activity and performance stability similar to Pt/C [12]. Previous studies [13–15] show that polypyrrole-modified carbon-supported cobalt hydroxide [$Co(OH)_2$–PPy/BP] catalysts have fairly high electroactivity toward ORR. However, the long-term

* Corresponding author. Tel./fax: +86 571 87953149.
E-mail address: zhoupengli@zju.edu.cn (Z.P. Li).

0378-7753/$ – see front matter © 2013 Elsevier B.V. All rights reserved.
http://dx.doi.org/10.1016/j.jpowsour.2013.01.175

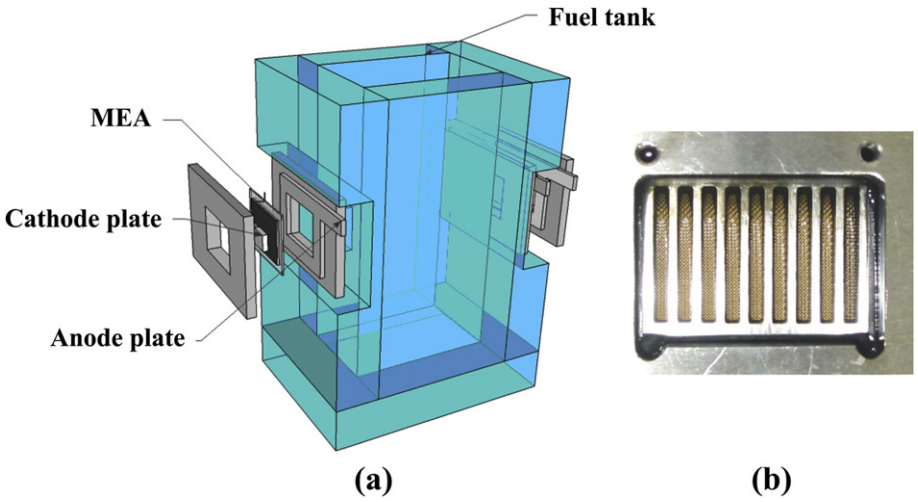

Fig. 1. (a) Schematic of the DBFC test module for performance degradation evaluation, and (b) top view of the single cell.

performance stability of these catalysts has not yet been evaluated. The effects of $Co(OH)_2$ on the performance stability of $Co(OH)_2$–PPy/BP catalyst are also unclear.

In this paper, we design and assemble a DBFC test set for performance degradation evaluation. The performance degradation behaviors of anode and cathode catalysts are investigated by electrode polarization measurements and physical characterizations. The effect of $Co(OH)_2$ in $Co(OH)_2$–PPy/BP on ORR during cell operation is discussed.

2. Experimental

Fig. 1 shows the test set for cell performance stability evaluation. Two single cells with a similar structure to a previously described microcell [16] were used. The cells were mounted 12 cm apart on the walls of a fuel tank to ensure the same environmental conditions. The prismatic fuel tank was made of acrylic and had a fuel reservoir capacity of 1.44 L ($L \times W \times H = 12 \times 6 \times 20$ cm^3). In the middle of the tank, two windows ($L \times W = 3.5 \times 3$ cm^2) facing each other were opened for anolyte transportation. Each single cell consisted of anode and cathode plates with slits for fuel and air transportation, and the entire anode–membrane–cathode assembly had an active area of 6 cm^2. To improve contact between the end plate and electrode, a hydrophobic gold-coated Ni grid (100 mesh) was welded to the end plate by spot welding, as shown in Fig. 1(b). The hydrophobic gold-coated Ni grid was prepared by dipping the gold-coated Ni grid in a polytetrafluorethylene (PTFE) emulsion (5 wt.%) followed by heating to 573 K under an argon atmosphere for 1 h after air drying.

The anode was prepared by pasting an anode ink onto a piece of Ni foam with a catalyst loading of 1 mg cm^{-2}. The anode ink was prepared by mixing the catalyst powders with water, ethanol, and Nafion solution (5 wt.%) or PTFE emulsion (5 wt.%) at a 1:3:3:7 mass ratio of catalyst:ethanol:Nafion solution (or PTFE emulsion):water. The cathode was prepared by painting a cathode ink onto a piece of hydrophobic carbon cloth. The cathode ink was prepared by mixing catalyst powder with water, ethanol, and PTFE emulsion (5 wt.%) at a 1:3:3:7 mass ratio of catalyst:ethanol:PTFE emulsion:water. The preparation procedure of $Co(OH)_2$–PPy/BP was as described in a previous study [13]. The electrolyte used to separate the anode from the cathode contained a cation exchange membrane (CEM): Nafion 112 membrane (Dupont) or anion exchange membrane (AEM): Neosepta AMX membrane (Tokuyama Soda). An alkaline $NaBH_4$ solution (5 wt.% $NaBH_4$–10 wt.% NaOH) was used as the fuel (anolyte). Cell performance polarization measurements and performance stability evaluation were conducted under ambient and passive conditions.

Electrode polarization measurements were conducted using the PFX2011S electrochemical workstation (Kikusui Electronics Corp.). A saturated calomel electrode (SCE) served as the reference electrode and was connected to the fuel tank with a salt bridge. The used fuel was replaced by fresh fuel at 96 h intervals.

The electrodes were subjected to cyclic voltammetry (CV) between −1.0 and 0.2 V (vs. SCE) at 25 °C with a scan rate of 50 mV s^{-1} in an alkaline O_2-saturated solution (0.1 mol L^{-1} KOH). The detailed preparation procedures of $Co(OH)_2$–PPy/BP electrodes for CV measurements are described elsewhere [15].

The microstructure of the synthesized catalysts was characterized by X-ray diffraction (XRD) using a Rigaku-D/MAX-2550PC diffractometer with Cu Kα radiation (λ = 1.5406 Å). The morphology of the anode was characterized by scanning electron

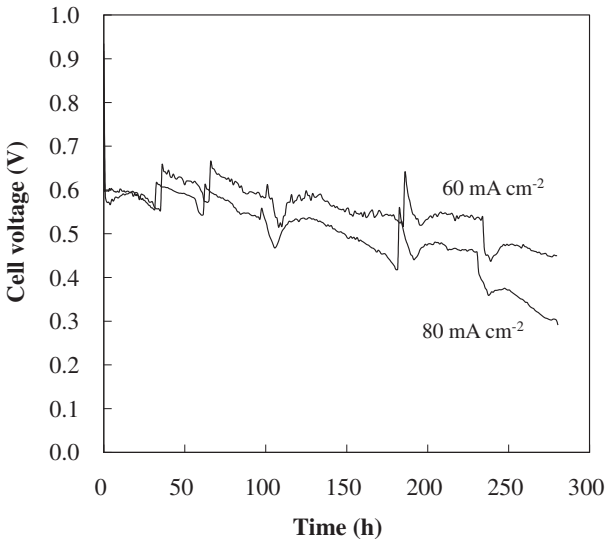

Fig. 2. Performance degradation of the DBFC using $Co(OH)_2$–PPy/BP as anode and cathode catalyst operating at a current density of 60 and 80 mA cm^{-2} under ambient conditions, respectively.

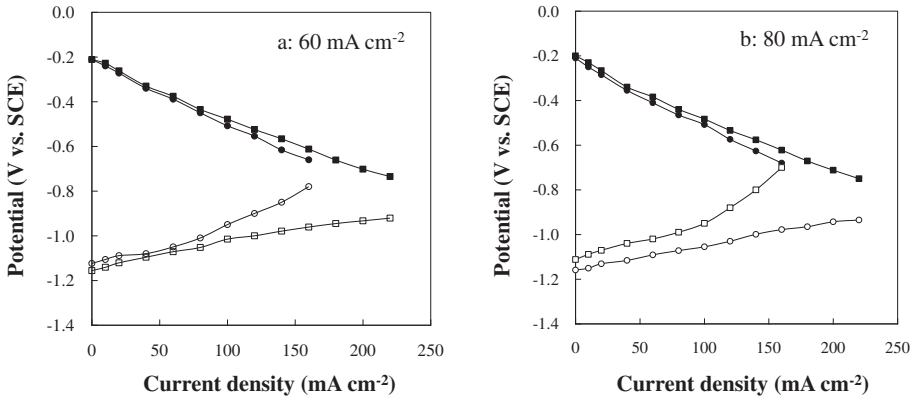

Fig. 3. Polarization behavior of $Co(OH)_2$–PPy/BP as anode and cathode catalyst after 280 h of operation at a current density of (a) 60 and (b) 80 mA cm^{-2} under ambient conditions, respectively.

microscopy (SEM). The chemical valence states of Co and N were investigated by X-ray photoelectron spectroscopy (XPS) using a PHI-5000C ESCA system (PerkinElmer Inc., USA). All spectra were referenced to the C ls level at 284.6 eV to correct the peak shift that occurred because of charge accumulation on the sample.

3. Results and discussion

A DBFC uses a CEM or AEM as the electrolyte to separate the anode from the cathode [17]. The DBFC using AEM (AEM–DBFC) produces water and borates at the anode side, and produces only OH^- at the cathode side. OH^- ions as the charge carrier move to the anode side during operation. Therefore, nothing remains at the cathode in the cathodic process. However, a DBFC using CEM (CEM–DBFC) produces borates at the anode side and NaOH solution at the cathode side [18].

Regardless of the DBFC configuration, gaseous hydrogen is produced from the hydrolysis and anodic reactions of borohydride [4], as shown in reactions (1) and (2), respectively.

$$BH_4^- + 2H_2O = BO_2^- + 4H_2 \quad (1)$$

$$BH_4^- + xOH^- = BO_2^- + (x-2)H_2O + (4-0.5x)H_2 + xe^- \quad (2)$$

Generally, borohydride hydrolysis is a zero-order reaction [19], i.e., its hydrogen evolution rate is a constant at a certain temperature. However, the hydrogen evolution rate r_e [standard volume of hydrogen V_H (liter) per minute] from an electrochemical reaction is proportional to the operation current I (ampere), as deduced from the electrochemical reaction (2):

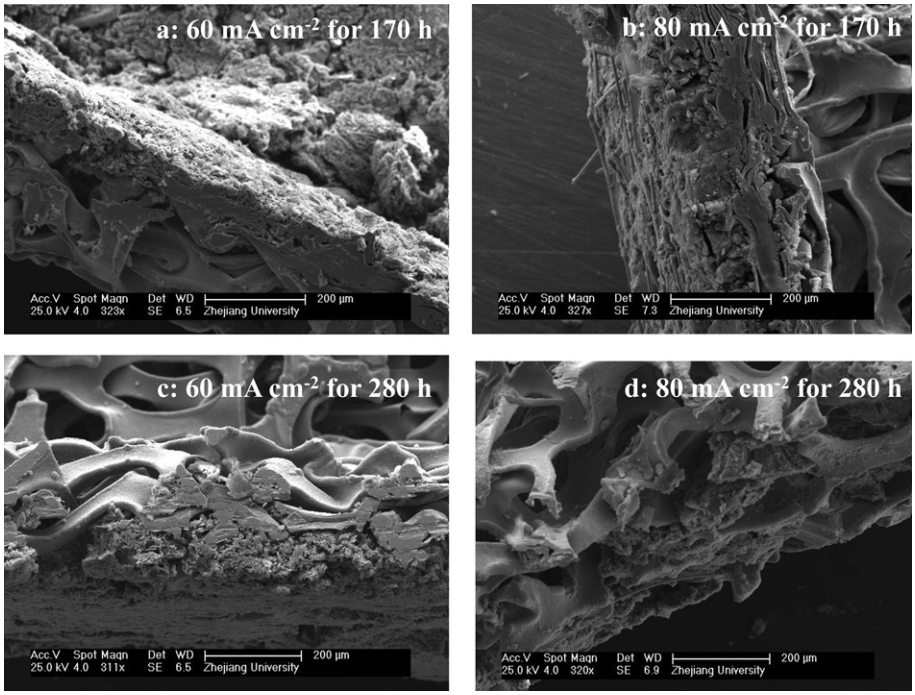

Fig. 4. Anode morphologies after 170 and 280 h of operation at a current density of 60 and 80 mA cm^{-2} under ambient conditions, respectively. The anode catalyst is $Co(OH)_2$–PPy/BP.

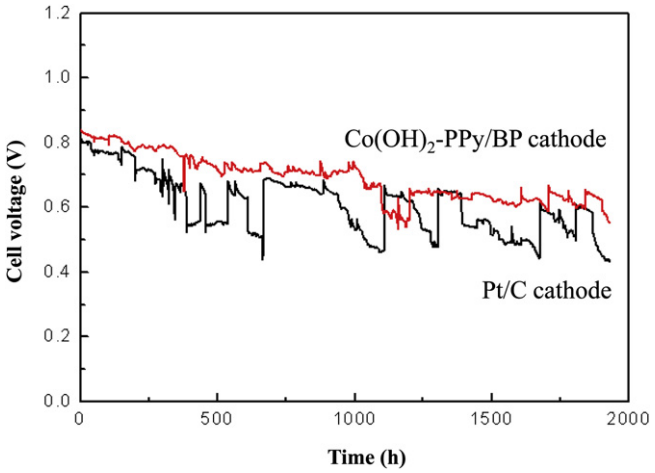

Fig. 5. Performance degradation of the DBFC using Ni–Pd/C as the anode catalyst, $Co(OH)_2$–PPy/BP or Pt/C as the cathode catalyst operating at a current density of 20 mA cm^{-2} under ambient conditions. The electrolyte is Nafion 112.

$$r_e = V_H/t = 22.4(4 - 0.5x)/t \quad \left(\text{L min}^{-1}\right) \tag{3}$$

Using Faraday's law yields

$$1/t = 60I/(xF) \quad \left(\text{min}^{-1}\right) \tag{4}$$

Considering Eqs. (3) and (4), the hydrogen evolution rate from the electrochemical reaction can be described as

$$r_e = 672(8 - x)I/(xF) \quad \left(\text{L min}^{-1}\right) \tag{5}$$

where F is the Faraday constant and x depends on the nature of anode catalyst [20–24] and cell operation conditions [25]. A higher DBFC performance leads to a larger operation current and higher hydrogen production rate at the anode, resulting in more severe catalyst erosion. Therefore, the depression of hydrogen evolution during operation is key to improving the DBFC performance stability.

3.1. Performance degradation of CEM–DBFC

Fig. 2 shows the performance degradation of the cell using $Co(OH)_2$–PPy/BP as the anode and cathode catalysts under different currents. Performance degradation rapidly proceeds under a large operation current. Electrode polarization measurements (Fig. 3) show that anode polarization more quickly increases than cathode polarization after 280 h of operation.

Increased operation current leads to accelerated hydrogen evolution, as described in Eq. (5). Furthermore, $Co(OH)_2$ in $Co(OH)_2$–PPy/BP is converted to metallic Co to catalyze borohydride hydrolysis. Consequently, when the cell operates at a higher current, more hydrogen bubbles are generated by borohydride hydrolysis and the electrochemical reaction erodes more anode catalysts from the anode substrate, as shown in the SEM images in Fig. 4. These results indicate that a faulty anode is a major cause of cell performance degradation.

Carbon-supported Pd in Ni anode with a suitable Nafion content can effectively depress hydrogen evolution during operation [4]. Fig. 5 shows the performance degradation of a DBFC using Ni–Pd/C as the anode catalyst and $Co(OH)_2$–PPy/BP or commercialized Pt/C as the cathode catalyst operated at a current density of 20 mA cm^{-2} under ambient conditions. The anode is separated from the cathode by a Nafion 112 membrane. Both anode and cathode polarizations in each cell are insignificantly deteriorated, as shown in Fig. 6(a) and (b). The performance stability of the cell using $Co(OH)_2$–PPy/BP as the cathode catalyst is similar to that of the cell using Pt/C.

As shown in Fig. 7, XRD analysis of $Co(OH)_2$–PPy/BP catalyst after 50 h of operation reveals that $Co(OH)_2$ is converted to CoOOH. Cell operation causes the binding energy of the Co $2p_{1/2}$ and $2p_{3/2}$ electrons to shift to a lower energy, as shown in Fig. 8(a), reconfirming that Co^{2+} in $Co(OH)_2$–PPy/BP is converted to Co^{3+} [26]. After 1000 h of operation, a very small amount of Co remains on the $Co(OH)_2$–PPy/BP catalyst based on XRD and XPS results. The XPS results demonstrate that the nitrogen content of $Co(OH)_2$–PPy/BP significantly decreases after 50 h of operation. A correlation of these XRD and XPS results with the performance stability evaluation reveals that small amounts of N and Co create sufficient catalytic sites for ORR, consistent with the suggestion of many researchers that a small amount of transit element plays a very important role in catalyzing ORR [27–29].

To understand the effect of $Co(OH)_2$ in $Co(OH)_2$–PPy/BP on ORR, $Co(OH)_2$–PPy/BP powders are treated by a dilute sulfuric acid solution (0.1 M) for 1 h to ensure that no crystalline $Co(OH)_2$ or CoOOH exists, as shown in Fig. 7. XPS analysis of the electron binding energy from 160 eV to 175 eV shows no sulfur signal. However, a weak peak of Co 2p is observed from 775 eV to 810 eV (Fig. 8(a)), suggesting that the sulfuric acid treatment removes $Co(OH)_2$ but not Co–Nx sites. The surface cobalt content of the sulfuric acid-treated $Co(OH)_2$–PPy/BP is similar to that of $Co(OH)_2$–PPy/BP after 1000 h of operation.

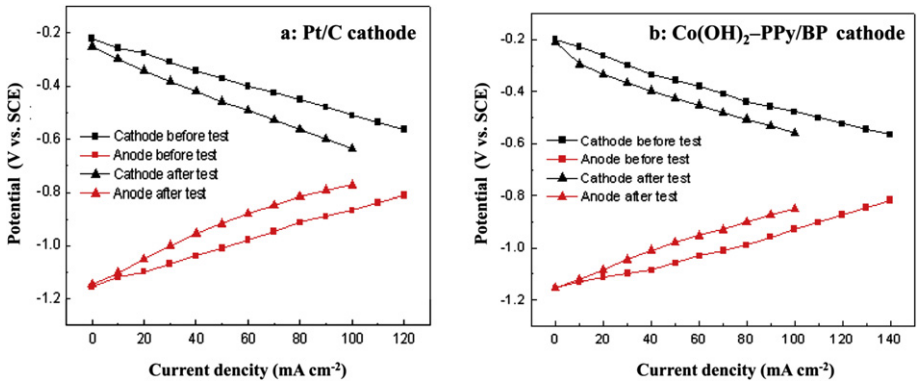

Fig. 6. Polarization behavior of (a) Pt/C and (b) $Co(OH)_2$–PPy/BP as the cathode catalyst after 1932 h of operation at a current density of 20 mA cm^{-2} under ambient conditions. The anode catalyst is Ni–Pd/C.

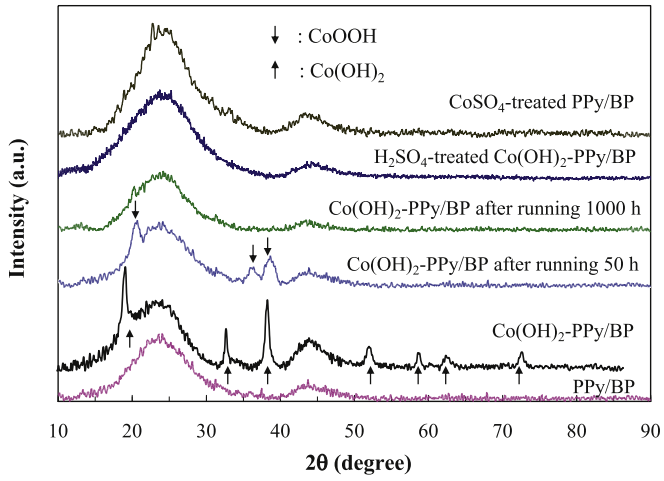

Fig. 7. XRD pattern of $Co(OH)_2$–PPy/BP catalyst after cell operation.

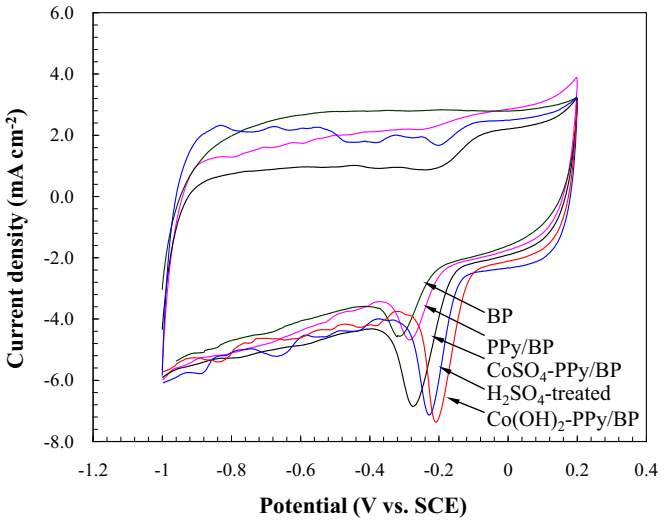

Fig. 9. Cyclic voltammograms of $Co(OH)_2$–PPy/BP, sulfuric acid-treated $Co(OH)_2$–PPy/BP, and $CoSO_4$-treated PPy/BP in an alkaline O_2-saturated solution (0.1 mol L^{-1} KOH).

The CV results show that the electroactivity of the sulfuric acid-treated $Co(OH)_2$–PPy/BP is similar to that of $Co(OH)_2$–PPy/BP, as shown in Fig. 9. Thus, sulfuric acid treatment leaves sufficient Co–N*x* sites, which are some of the major catalytic sites for ORR [29,30]. This result indicates that the existence of Co–N*x* site is more important than the formation of CoOOH, although CoOOH possesses electroactivity for ORR [31]. This phenomenon is understandable because Co and N in Co–N*x* catalyzes ORR in the form of radicals, whereas $Co(OH)_2$ (or CoOOH) catalyzes ORR in the form of crystals (much larger than radicals). The inner Co in the CoOOH or $Co(OH)_2$ crystal is inactive toward ORR.

Considerable efforts have been exerted to investigate the effects of trace Co and N contents in acid-treated $Co(OH)_2$–PPy/BP by energy dispersive X-ray spectroscopy, X-ray fluorescence spectrometry, and XPS. However, these quantitative analyses have not produced consistent and reliable results. Thus, in the present study, PPy/BP is doped with a trace amount of Co by a chemical method to verify the effect of trace Co content on ORR.

PPy-modified BP carbon (PPy/BP = 0.7 g) was dipped into a $CoSO_4$ solution (100 mL, 12 mmol L^{-1}) for 12 h at 60 °C. Compared with PPy/BP, no significant change in the catalyst structure is observed through XRD analysis, as shown in Fig. 7. Similar to the sulfuric acid-treated $Co(OH)_2$–PPy/BP, very few Co is detected on the surfaces of the $CoSO_4$ solution-treated PPy/BP ($CoSO_4$–PPy/BP) by XPS analysis, as shown in Fig. 8(a). CV results indicate that the electroactivity of $CoSO_4$–PPy/BP is similar to that of $Co(OH)_2$–PPy/BP and sulfuric acid-treated $Co(OH)_2$–PPy/BP, and better than that of BP- or PPy-modified BP (PPy/BP), as shown in Fig. 9.

The approximate Koutechy–Levich (K–L) is useful for estimating the number of electrons transferred (n) per O_2 molecule through ORR on powder catalyst [15]:

$$j^{-1} = j_k^{-1} + \left\{0.62nFC_0D_0^{2/3}\nu^{-1/6}\omega^{1/2}\right\}^{-1} \quad (6)$$

where j_k is the kinetically apparent limiting current density, ω is the angular frequency of rotation, and F is the Faraday constant. The O_2 concentration (C_0), diffusion coefficient (D_0) of O_2 in 0.1 mol L^{-1} KOH solution, and kinematic viscosity (ν) of the 0.1 mol L^{-1} KOH solution are 1.15 × 10^{-3} mol L^{-1}, 1.95 × 10^{-5} cm^2 s^{-1}, and 0.008977 cm^2 s^{-1}, respectively [32]. Fig. 10 shows the rotating disk electrode (RDE) voltammograms of $Co(OH)_2$–PPy/BP, $CoSO_4$–PPy/BP, and sulfuric acid-treated $Co(OH)_2$–PPy/BP recorded between −0.85 and −0.15 V (vs. SCE) at a scan rate of 10 mV s^{-1} as well as rotation rates of 300, 400, 600, 800, and 1250 rpm in a 0.1 mol L^{-1} KOH solution saturated with O_2 at 25 °C, respectively. Fig. 11 presents the K–L plots related to the RDE CV results of $Co(OH)_2$–PPy/BP, $CoSO_4$–PPy/BP, and sulfuric acid-treated $Co(OH)_2$–PPy/BP at 0.5, 0.6, and 0.7 V, respectively. Table 1 summarizes the effects of doping PPy/BP with $CoSO_4$ and the sulfuric acid washing of $Co(OH)_2$–PPy/BP on the number of electrons transferred (n), as well as the kinetically apparent limiting current density (j_k) values. $CoSO_4$–PPy/BP exhibits equivalent n and j_k values of $Co(OH)_2$–PPy/BP, revealing that cobalt compounds exert

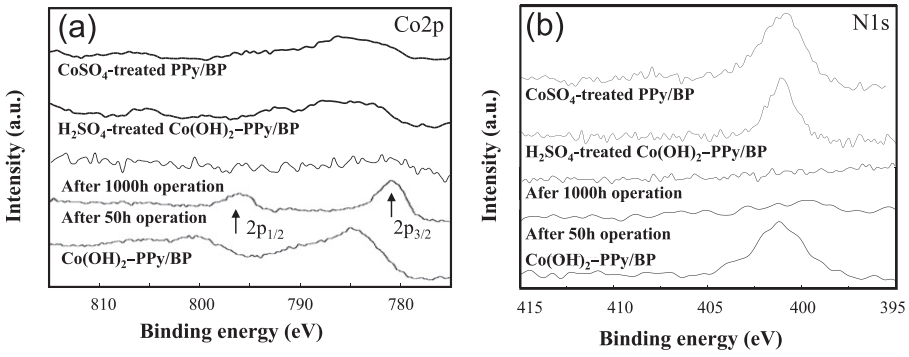

Fig. 8. Normalized X-ray photoemission spectra of (a) Co2p and (b) N1s for $Co(OH)_2$–PPy/BP after operation.

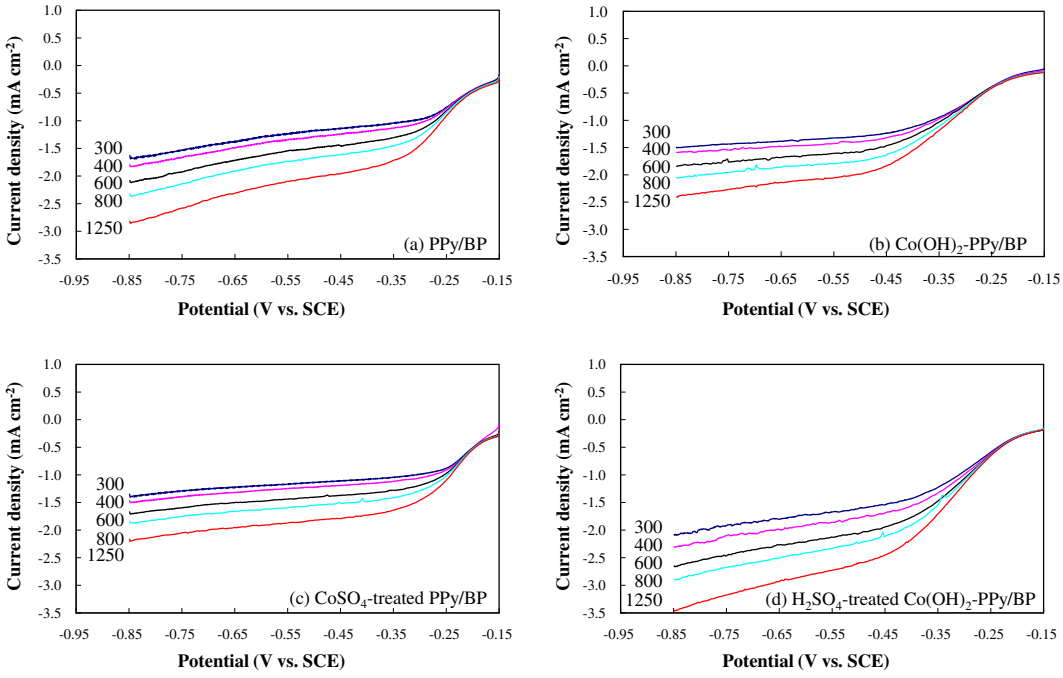

Fig. 10. Rotating disk electrode voltammograms of (a) PPy/BP, (b) $Co(OH)_2$–PPy/BP, (c) $CoSO_4$–PPy/BP, and (d) sulfuric acid-treated $Co(OH)_2$–PPy/BP at a scan rate of 10 mV s^{-1} and rotation rates of 300, 400, 600, 800, 1250 rpm in 0.1 mol L^{-1} KOH saturated with O_2 at 25 °C.

the same enhancement effect on ORR because of the formation of Co–N*x* for ORR [15] whether in the form of salt or base. The subsequent sulfuric acid treatment of $Co(OH)_2$–PPy/BP results in further improved ORR activity (higher values of *n* and j_k), implying that sulfuric acid treatment does not damage the Co–N*x* site of $Co(OH)_2$–PPy/BP but creates some new sites for ORR. Further detailed investigations are required to explain this phenomenon.

Based on the aforementioned experimental results and discussion, the high performance stability of $Co(OH)_2$–PPy/BP to ORR can be attributed to the existence of trace Co and N in $Co(OH)_2$–PPy/BP catalyst to form sufficient Co–N*x* sites for ORR.

3.2. Performance degradation of AEM–DBFC

Compared with the CEM–DBFC, the AEM–DBFC has a harmonious cell configuration because only water and borates are generated at the anode side during cell operation, consistent with the nature of DBFC. However, unlike the CEM–DBFC that generates

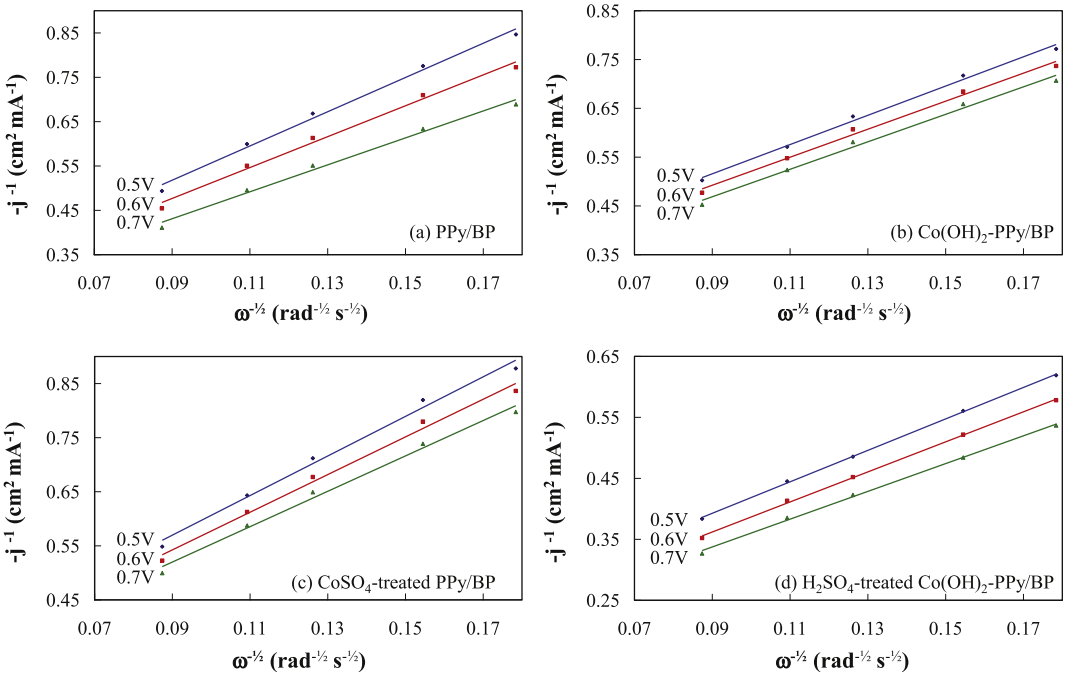

Fig. 11. Koutechy–Levich plots related to the rotating disk electrode cyclic voltammograms of $Co(OH)_2$–PPy/BP, $CoSO_4$–PPy/BP, and sulfuric acid-treated $Co(OH)_2$–PPy/BP at 0.5, 0.6, and 0.7 V.

Table 1
Effects of doping PPy/BP with $CoSO_4$ and sulfuric acid washing of $Co(OH)_2$–PPy/BP on the number of electrons transferred (n) and kinetically apparent limiting current density (j_k).

	PPy/BP	$Co(OH)_2$–PPy/BP	$CoSO_4$–PPy/BP	H_2SO_4 treated $Co(OH)_2$–PPy/BP
n	2.6	3.2	2.6	3.8
$-j_k$ (mA cm^{-2})	2.0	4.3	4.3	6.9

alkaline solution at the cathode, air humidification is necessary to run the AEM–DBFC because OH^- transportation from the cathode side to the anode side requires water drag. Therefore, the AEM–DBFC has to be run under cathode humidification at a high temperature, such as 60 °C. However, increased DBFC operation temperature leads to accelerated borohydride hydrolysis. A hydrophobic anode structure using PTFE as the binder is suggested to control the contact of catalyst to anolyte ($NaBH_4$ solution) and, subsequently, to depress hydrogen evolution during operation. Fig. 12 shows the hydrogen evolution behavior of the anode using Nafion or PTFE as the binder. The anode using PTFE as the binder demonstrates much lower hydrogen evolution rate than that using Nafion as the binder. Fig. 13 shows the performance degradation of the AEM–DBFC using this hydrophobic anode and the Neosepta AMX membrane at a current density of 40 mA cm^{-2} and at 60 °C. The AEM–DBFC exhibits high performance stability similar to CEM–DBFC, revealing that the Neosepta AMX membrane has comparable anti-degradation ability to Nafion membrane. $Co(OH)_2$–PPy/BP in the AEM–DBFC has comparable performance stability to that in CEM–DBFC.

However, the AEM–DBFC with the hydrophobic anode shows very chaotic cell voltage during initial operation (Fig. 13) compared with the CEM–DBFC with hydrophilic anode (Fig. 5). When hydrogen generated by borohydride hydrolysis or/and electrooxidation begins to fill the cavities of the hydrophobic porous anode during operation, the ionic conductivity of the anode decreases such that cell voltage drops. Hydrogen electrooxidizes at higher potentials than BH_4^-. With decreased cell voltage (increased anode potential), hydrogen in the anode starts to electrooxidize. Subsequently, the anolyte refills these cavities to improve the anode's ionic conductivity and the cell voltage recovers. Within a certain operation period, the hydrophobic anode yields water affinity (similar to the alkaline treatment of PTFE to gain water affinity) such that the anode's ionic conductivity stabilizes. Therefore, the AEM–DBFC with the hydrophobic anode shows a relatively stable performance after initial operation. Three-dimensional electrodes are considered as able to avoid the chaotic performance of hydrophobic anodes because three-dimensional

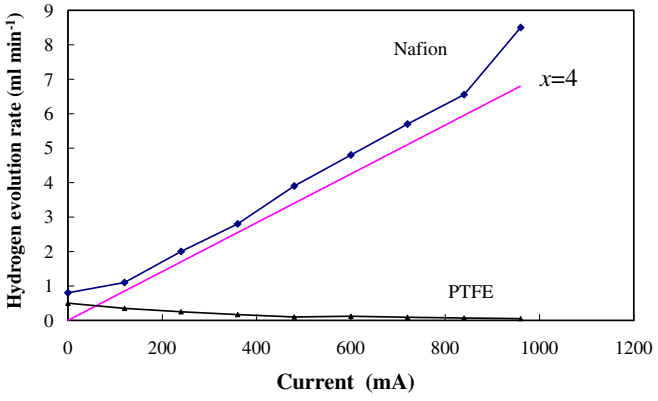

Fig. 12. Hydrogen evolution behavior of the anode using Nafion or PTFE as the binder.

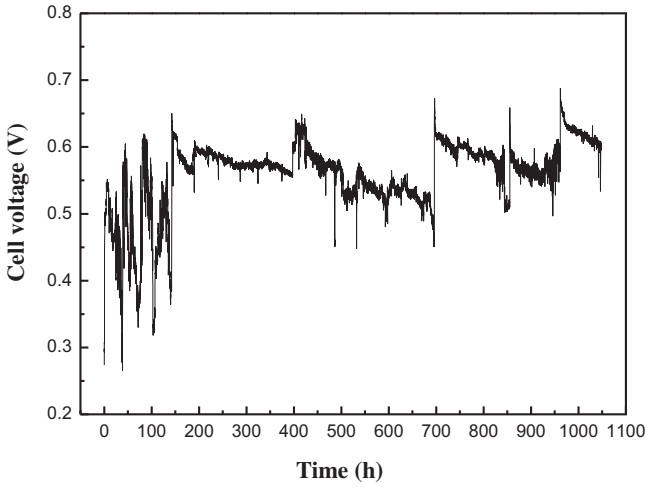

Fig. 13. Performance degradation of the AEM–DBFC using a hydrophobic anode and Neosepta AMX membrane as the electrolyte at a current density of 40 mA cm^{-2} and at 60 °C.

electrodes stabilize the ionic conductivity of anodes by improving hydrogen transport [8].

After more than 1000 h of operation, the electrodes are difficult to peel off from the Neosepta AMX membrane. From the original light yellow, the membrane becomes brown. The used membrane loses some amount of tensile strength and becomes relatively brittle. Thus, AMX membranes are not highly suitable for DBFCs running at a high temperature.

4. Conclusions

In this study, a faulty anode caused by catalyst erosion from the substrate is the key factor affecting DBFC performance degradation. The depression of hydrogen evolution slows down the anode catalyst erosion to stabilize DBFC performance. Improvement of the anode structure to avoid catalyst erosion using a three-dimensional porous anode is the next target of our group to enhance DBFC performance stability.

The DBFC using Ni–Pd/C as the anode catalyst and the PPy-modified carbon-supported $Co(OH)_2$ [$Co(OH)_2$–PPy/BP] as the cathode catalyst shows high performance stability. Under the depression of hydrogen evolution, the DBFC using either AEM or CEM demonstrates long-term reliable performance stability.

The performance stability of $Co(OH)_2$–PPy/BP is similar to that of commercialized Pt/C. The cooperative interaction among Co, N, and C is the key factor affecting the performance stability of $Co(OH)_2$–PPy/BP cathode.

Acknowledgments

This work is financially supported by the National Natural Science Foundation of China, Grant Nos. 20976156, 50971114, 21276229, 51271164 and 21006090; the Qian Jiang Talents Project of Science Technology Department of Zhejiang Province, Grant No. 2012R10058; the Zhejiang Provincial Natural Science Foundation of China, Grant No. Z4110126; the Doctoral Fund from the Education Ministry of China (20100101110042); and the Fundamental Research Funds for the Central Universities.

References

[1] D.M.F. Santos, C.A.C. Sequeira, Renew. Sustain. Energy Rev. 15 (2011) 3980–4001.

[2] B.H. Liu, Z.P. Li, J. Power Sources 187 (2009) 291–297.
[3] J. Ma, N.A. Choudhury, Y. Sahai, Renew. Sustain. Energy Rev. 14 (2010) 183–199.
[4] Z.P. Li, B.H. Liu, J.K. Zhu, S. Suda, J. Power Sources 163 (2006) 555–559.
[5] B.H. Liu, Z.P. Li, J.K. Zhu, S. Suda, J. Power Sources 183 (2008) 151–156.
[6] C. Kim, K.-J. Kim, M.Y. Ha, J. Power Sources 180 (1) (2008) 154–161.
[7] C. Kim, K.-J. Kim, M.Y. Ha, J. Power Sources 180 (1) (2008) 114–121.
[8] V.W.S. Lam, D.C.W. Kannangara, A. Alfantazi, E.L. Gyenge, J. Power Sources 212 (2012) 57–65.
[9] G.J. Wang, Y.Z. Gao, Z.B. Wang, C.Y. Du, G.P. Yin, Electrochem. Commun. 12 (2010) 1070–1073.
[10] B.H. Liu, S. Suda, J. Power Sources 164 (2007) 100–104.
[11] H. Cheng, K. Scott, K. Lovell, Fuel Cells 6 (2006) 367–375.
[12] H. Cheng, K. Scott, J. Electroanal. Chem. 596 (2006) 117–123.
[13] H.Y. Qin, Z.X. Liu, S.J. Lao, J.K. Zhu, Z.P. Li, J. Power Sources 195 (2010) 3124–3129.
[14] H.Y. Qin, S.J. Lao, Z.X. Liu, J.K. Zhu, Z.P. Li, Int. J. Hydrogen Energy 35 (2010) 1872–1878.
[15] H.Y. Qin, K.N. Zhu, L.Q. Ye, Z.P. Li, J. Power Sources 208 (2012) 203–209.
[16] B.H. Liu, Z.P. Li, K. Arai, S. Suda, Electrochim. Acta 50 (2005) 3719–3725.
[17] Jung-Ho Wee, J. Power Sources 155 (2006) 329–339.
[18] Z.P. Li, B.H. Liu, K. Arai, S. Suda, J. Electrochem. Soc. 150 (2003) A868–A872.
[19] B.H. Liu, Z.P. Li, J. Power Sources 187 (2009) 527–534.
[20] L.C. Nagle, J.F. Rohan, Int. J. Hydrogen Energy 36 (2011) 10319–10326.
[21] C. Ponce de León, A. Kulak, S. Williams, I. Merino-Jiménez, F.C. Walsh, Catal. Today 170 (2011) 148–154.
[22] G. Rostamikia, M.J. Janik, Energy Environ. Sci. 3 (2010) 1262–1274.
[23] X.Y. Geng, H.M. Zhang, Y.W. Ma, H.X. Zhong, J. Power Sources 195 (2010) 1583–1588.
[24] B. Molina Concha, M. Chatenet, Electrochim. Acta 54 (2009) 6130–6139.
[25] B.H. Liu, Z.P. Li, S. Suda, Electrochim. Acta 49 (2004) 3097–3105.
[26] A.C. Tuan, J.D. Bryan, A.B. Pakhomov, V. Shutthanandan, S. Thevuthasan, D.E. McCready, D. Gaspar, M.H. Engelhard, J.W. Rogers, K. Krishnan, D.R. Gamelin, S.A. Chambers, Phys. Rev. B 70 (5) (2004) 054424.
[27] M. Kobayashi, H. Niwa, Y. Harada, K. Horiba, M. Oshima, H. Ofuchi, K. Terakura, T. Ikeda, Y. Koshigoe, J. Ozaki, S. Miyata, S. Ueda, Y. Yamashita, H. Yoshikawa, K. Kobayashi, J. Power Sources 196 (2011) 8346–8351.
[28] W. Yang, T.P. Fellinger, M. Antonietti, J. Am. Chem. Soc. 133 (2011) 206–209.
[29] Z.P. Li, Z.X. Liu, K.N. Zhu, Z. Li, B.H. Liu, J. Power Sources 219 (2012) 163–171.
[30] G. Wu, M.A. Nelson, N.H. Mack, S.G. Ma, P. Sekhar, F.H. Garzon, P. Zelenay, Chem. Commun. 46 (2010) 7489–7491.
[31] Z.X. Liu, Z.P. Li, H.Y. Qin, B.H. Liu, J. Power Sources 196 (2011) 4972–4979.
[32] D. Zhang, D. Chi, T. Okajima, T. Ohsaka, Electrochim. Acta 52 (2007) 5400–5406.